Proceedings of the
International Conference on Mechanical Engineering 2011
(ICME2011) 18-20 December 2011, Dhaka, Bangladesh

ICME 11-AM-001

INTERFACIAL FRACTURE STRENGTH MEASUREMENT OF BONE-PMMA CEMENT CONSTRUCTS

Morshed Khandaker and Yanling Li

Department of Engineering and Physics, University of Central Oklahoma, Edmond, OK 73034, USA

ABSTRACT

The interfacial mechanics at the bone-implant interface is a critical issue for implant fixation and the filling of bone defects created by tumors and/or their excision. The present study is based on the hypothesis that the differences of the surface roughness at bone/ implant interface due to incorporation of micro and nano size MgO particle additives may have significant influence on the quality of bone/implant union. This research studied poly Methyl MethAcrylate (PMMA) bone cement with and without MgO additives as different implant materials. The aims of this research were to: to quantify elastic properties of bone cement specimens, and to determine whether inclusion of MgO particles with PMMA has any influence on the interface strength between bone and PMMA. This study found that the mean interface strength for bone-PMMA is significantly less than the mean interface strengths of bone-PMMA with microsize MgO particles and bone-PMMA with nanosize MgO particles.

Keywords: PMMA, MgO, Bone cement, Interface Strength, Additives, Orthopedics.

1. INTRODUCTION

The most challenging issue associated with commercially available PMMA bone cements such as Cobalt (Biomet, Inc.), Simplex (Stryker, Inc.), Palacos (Heraeus company) for the application of total joint replacement is their poor osseointegration (incorporation of the cement with surrounding bone tissues) [1]. Problems about infection and loosening of the bone cements at the bone-cement interface have been reported in literature [2]. One way to reduce infection and loosening would be to promote osteoblast cell growth around the cemented surfaces. Such cells can eliminate contact between the bone and the environment and restricting contamination at the cemented prosthetic joint. Another way to reduce loosening would be to increase mechanical interlock between bone and cement [3, 4]. This can be done by enhancing the surface roughness of the PMMA cement. Several research groups found improvement of PMMA bone cements surface roughness properties by incorporating different kinds of additives materials with the PMMA cement [2, 5-8]. Recently researchers found MgO, Silver, hydroxyapatite nanoparticle filler materials improve bone healing properties of conventional PMMA bone cements [2, 5, 6, 8-10]. The mechanism of bonding of bone with these additives incorporated PMMA bone cement may be different from bonding of bone with PMMA without these additives. The influences of the inclusion of these additives with bone cement on the bonding stress between natural bone and cements were not investigated yet. Such study is required for the suitability of using the additives with the bone cement. Ricker *et al*.[8] research on PMMA cement showed increased surface roughness, and enhanced cell adhesion of mouse osteoblast cell on PMMA due to the inclusion of MgO additives with PMMA. The suitability of incorporating MgO additive with bone cement requires complete understanding of the failure mechanism of bone/MgO additives incorporated bone cement interfaces. No study has been conducted to evaluate the effect of MgO additives surface roughness on the mechanical integrity between bone and PMMA cement with MgO additives. In this present study, three kinds of bone cement were investigated. Cobalt™ HV bone cement (referred in this literature as CBC), a commercial orthopedic bone cement, was used as control PMMA bone cement. Micro and nano particle size MgO additives were mixed with CBC to prepare the other kinds of specimen. Cobalt™ HV bone cement with 36 µm mesh size MgO particle was referred in this literature as mCBC. Cobalt™ HV bone cement with 22 nm mesh size MgO particle was referred in this literature as nCBC. The goal of this research was to determine whether inclusion of MgO particles with PMMA bone cement has any influence on the bonding strength between bone and PMMA cement.

The present study is based on the hypothesis that the differences of the surface condition at bone/ bone cement interface due to additive materials particle size may have significant influence on the quality of bone/bone cement union. The scopes of works for this research were: (1) to quantify elastic properties of bone cement specimens, (2) to determine whether inclusion of MgO particles with

PMMA has any influence on the interface strength between bone and CBC..

Evex SEM tensile stage was used in the study. Two groups of specimens were prepared: dogbone (CBC, mCBC, nCBC) and bilayer specimens (bone-CBC, bone-mCBC, and bone-nCBC). Tension tests were conducted on the first group of specimens to quantify the Young's modulus and Poisson's ratio of different kinds of cement specimens. Tension tests were conducted on the second group of specimens to quantify the MgO additive particle size effect on the interface fracture toughness of different bilayer specimens.

2. MATERIALS AND METHODS

2.1 Sample Preparation

According the Biomet, Inc (manufacturer of CBC) recommendation, 10 grams of poly Methyl MethAcrylate (PMMA) beads was as added to 5 ml of MMA monomer to prepare the CBC specimen. To prepare mCBC and nCBC specimen, 10 % (w/w) of the 36 µm and 22 nm sizes MgO powders were mixed with PMMA beads, respectively. The mixer was added into the MMA monomers maintaining the same solid:liquid ratio of 2 : 1 for the preparation of the respective samples. Both 36 µm and 22 nm sizes MgO powders were purchased from Sigma-Aldrich.

In order to cure the bone cement composition, a mold was designed using ProE solid modeling software (Fig. 1(a)). The designed parts were fabricated using CNC machine and dimension elite 3D printer (Fig. 1(b)). The top plate has extruded section that closely fit to the hole of the bottom plate. One of the side blocks of the mold has a 250 µm slot to allow a 220 µm plastic sheet to move through the mold chamber. Two side blocks and one side block with slot were made using 3D printer. The 3D printer used tough ABS plastic for fabricating the blocks. The rest of the pieces in the mold were made of acrylic. A C-shape clamp was used to secure the position of side blocks during the curing of the samples. Glass slides were glued at the interior boundaries of the mold chamber to avoid contact of PMMA with acrylic and ABS plastic during curing.

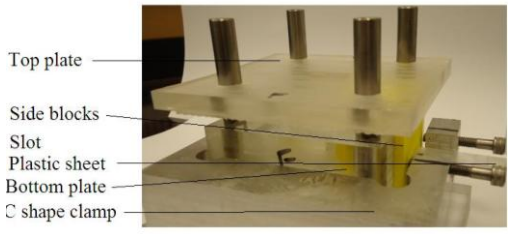

Fig. 1 Fabricated mold used for the preparation of bone cement specimens.

The mold as shown in Fig. 1(b) was to prepare different kinds of cement blocks of size (22×12×8) mm. Two side blacks without slot were used to prepare the cement blocks. Cement composition of interest was poured on the mold chamber during doughy phase. A set of weights were placed on the top plate to apply 80 kPa pressure (clinically applied pressure during orthopedic surgeries [11]) to the samples during the entire curing period. The cured blocks were milled to ASTM standards bowtie tensile specimen. The length and width of gage is Fig 2 shows the prepared CBC, mCBC and nCBC samples.

(a) (b) (c)

Fig 2. Fabricated ASTM 399 standard (a) CBC, (b) mCBC and (c) nCBC dog bone cement samples for the measurement of tension modulus and Poisson's ratio of the respective samples.

To prepare the different bone-PMMA cement specimens as shown in Fig 3(b), bone samples were extracted from the mid-diaphyses of fresh bovine femoral shaft obtained from a local abattoir. The femoral shafts were cut longitudinally into two blocks. Each block was milled down to a thickness of 2 mm. Bone coupons of (20×100~200×2) mm dimension were prepared from each block. The bone coupons was cut further to (22×12×2) dimension samples for bone-cement specimens using (4×0.012×$^1/_2$) in. diamond wafering blade in a low-speed saw cutter (Buehler isomet 11-1180-100). Wet bone blocks were placed on the aluminum bar in the mold chamber. A side black without slot and a side black with slot were mounted in the mold. A plastic sheet (100mm×12mm×200µm) was inserted through the side blocks in such a way that the sheet covered (12×6) mm area of the bone surface. The cement composition of interest was prepared to create up to 2 mm cement layer on the top bone. The cement were poured on top of the bone and pressed by top plate. A set of weights equivalent to 80 kPa pressure (clinically applied range [11]) were applied to the samples during the curing process. The pressure was initiated at exactly three minutes after the onset of mixing and was sustained throughout the curing period. After curing the plastic sheet was pull manually. Bone-cement sample were carefully glued with two ABS plastic holders made using 3D printer. Fig 4(b) shows a prepared bone-cement sample. The bone-cement samples were wrapped with wet Kim wipe papers to keep the bone sample wet before experiment.

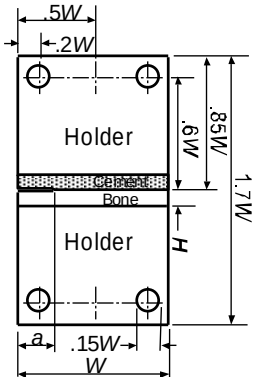

Fig 3. Schematic diagram of Bone-Cement bilayer specimen.

2.2 Experiments

2.2.1Measurements of the Elastic (E, N) Properties of Different Cement Samples

Tension test were conducted on the dogbone cement specimens at room temperature using Evex SEM tensile tester (300 N load cell) as shown in Fig 4(a). The specimens were mounted on the serrated clamp in the test stage. Two Micro-miniature displacement variable reluctant transducers (DVRTs) (MicroStrain, Inc) were glued on the specimen as shown in Fig 3(a). DVRTs were used to measure axial displacement during tension. Nikon SMZ stereomicroscope with DS-Fi1 camera and Nikon NIS BR software was used to sequentially capture images at 10 sec interval. The captured images was analyzed to measure transverse displacement during tension. All specimens were loaded with a loading rate equal to 3 μm/s until load-displacement curve starts to become non-linear. The load and displacement from Evex tensile stage, axial displacement from DVRT and visualization of transverse deformation were continuously recorded using Evex nanoanalysis, LabView 10.0 and Nikon NIS BR softwares, respectively. The stress in the sample was calculated at any time by dividing the load over the cross-sectional area. The axial displacement in the sample was measured directly from LabView data at any time by subtracting the displacement from the initial displacement. The strain in the sample was calculated at any time by dividing this displacement over by the DVRT gauge length. The slope of the stress-strain curve in the elastic region was used to calculate the tension modulus, *E*. The transverse displacement in the sample was measured directly from recorded Nikon sequential images at 10 sec interval by subtracting the dimension of the width of the sample from the initial width. The ratio of the transverse strain and axial strain, where load-displacement curve starts to become non-linear, was used to calculate the Poisson's ratio, υ.

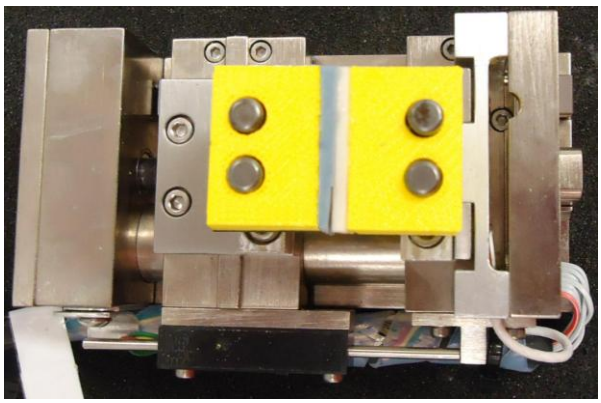

Fig 4. Evex tensile test stage with bone-PMMA cement sample.

2.2.2 Measurements of the Interface Fracture Toughness of Different Bone-Cement Samples

Tension test were conducted on the bone - cement bilayer specimens at room temperature using Evex SEM tensile tester (300 N load cell) as shown in Fig 4. The specimens were mounted on the tension clamp rod in the test stage. All specimens were loaded with a loading rate equal to 3 μm/s. The load and displacement were continuously recorded until the failure of the specimens using Evex nanoanalysis software. The bone-cement specimen kept wet during the experiment.

2.3 Data Analysis

Interfacial fracture toughness of bone and PMMA cement were calculated using [12]:

$$K_C = \frac{\lambda^{\psi} P_C Y \sqrt{\pi a}}{BW} \tag{1}$$

where K_C is the interfacial fracture toughness, P_C is the critical load that breaks the interface between bone and cement, λ is a scale factor determined by elastic properties of the bone and PMMA cement materials, ψ is a correction factor which is a function of the normalized interlayer thickness h/W, B is the thickness of specimen, W is the specimen width, and the remaining parameter Y is a constant determined by W and initial crack length a. Parameter λ can determined using:

$$\lambda = \sqrt{\frac{1-\alpha}{1-\beta^2}} \tag{2}$$

where α and β are Dundurs parameters, which estimate the elastic mismatch across the interface, are given by [12]:

$$\alpha = \frac{E_1\left(1-\nu_2^2\right) - E_2\left(1-\nu_1^2\right)}{E_1\left(1-\nu_2^2\right) + E_2\left(1-\nu_1^2\right)}$$
$$\beta = \frac{E_1\left(1-\nu_2-2\nu_2^2\right) - E_2\left(1-\nu_1-2\nu_1^2\right)}{2E_1\left(1-\nu_2^2\right) + 2E_2\left(1-\nu_1^2\right)} \tag{3}$$

where E_1, E_2, and ν_1, ν_2 are elastic moduli and Poisson's ratios of the PMMA cements and bone, respectively. Tension tests were conducted on different kinds of dogbone cement specimen to find E_1 and ν_1. In Eq. (1), ψ can be calculated as [12]

$$\psi = e^{5.056(h/W)^{0.777}} \tag{4}$$

In Eq. (1), *Y* is function of *a* and *W* can be calculated using [12]:

$$Y = \frac{1}{1-\rho}\sqrt{\frac{0.26 + 2.65\frac{\rho}{1-\rho}}{1 + 0.55\frac{\rho}{1-\rho} - 0.08\left(\frac{\rho}{1-\rho}\right)^2}} \tag{5}$$

where ρ=*a*/*W*.

2.4 Statistical Analysis

Interfacial fracture toughness of different samples was analyzed statistically using ANOVA techniques in SAS version 9.1. For all statistical analysis, statistical significance was considered as $P<0.5$.

3. RESULTS AND DISCUSSION

3.1 Elastic Properties (Tension Modulus and Poisson's Ratio) of Cement Specimens

Our studies found a difference of the stress-strain curve among different kinds of bone cement specimens (Fig 5). Table 1 reports the tension modulus and Poisson's ratio of different kinds of cements.

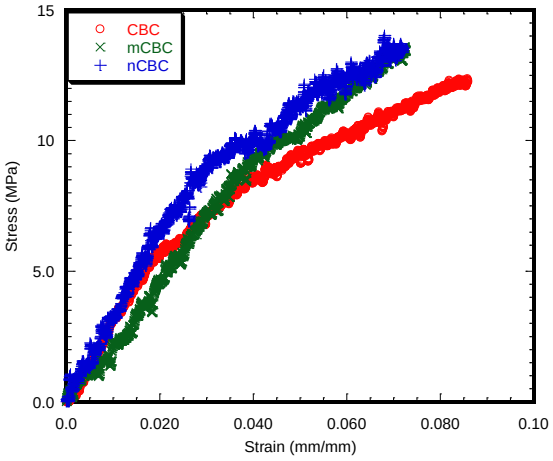

Fig 5. Difference of stress vs. strain among CBC, mCBC and nCBC specimens.

Table 1: Tension modulus and Poisson's ratio of different kinds of bone cement specimen

Specimen type	No of specimen	Young's modulus, E_1 (Mpa)	Poisson's ratio, v_1
CBC	2	262.11 ± 8.39	0.267 ± 0.001
mCBC	2	264.49 ± 11.24	0.278 ± 0.038
nCBC	2	326.54 ± 2.54	0.421 ± 0.032

3.2 Effect of Mgo Particle Size on the Interface Strength Between Bone and Cements

Figure - 6 compares the load-displacement curves of various bone-cement specimens. The load-displacement response of bone-CBC specimen specimens is characterized as initially elastic response, followed by a short inelastic region and then sudden failure of the specimen.

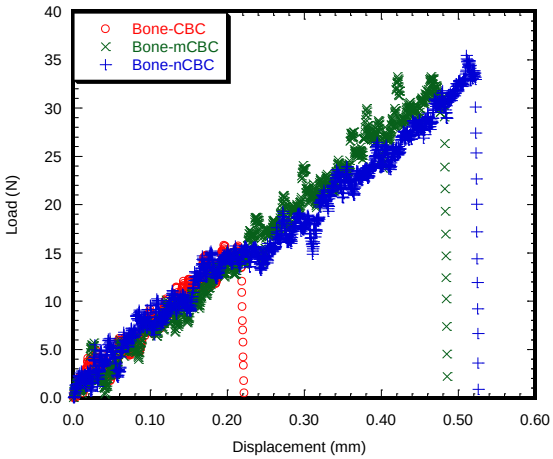

Fig 6. Load versus displacement graphs of (a) bone-CBC, (b) bone-mCBC and (c) bone-nCBC specimens.

Table 2 compares the interface fracture toughness of various kinds of bone and cement specimen. Results show MgO additives particle size has significant effects on the interface fracture toughness of bone-CBC specimens ($p<0.0001$). Specifically, the mean interface strength for bone-CBC is significantly less than the mean interface strengths of either of the other groups. There are no statistical significant differences of the mean interfacial strength between bone-mCBC and bone-nCBC

Table 2: Interfacial fracture toughness of various kinds of bone-cement specimens

Specimen type	No of specimen	Average width, W (mm)	Average height, H (mm)	Average thickness, B (mm)	Average crack length, a (mm)	Interface fracture toughness, K_{IC} (KPa.m$^{1/2}$)
Bone-CBC	6	21.48 ± 0.04	1.77 ± 0.16	11.94 ± 0.03	5.38 ± 0.15	9.57 ± 2.19
Bone-mCBC	6	21.65 ± 0.29	1.67 ± 0.15	11.95 ± 0.04	5.33 ± 0.18	24.54 ± 4.91
Bone-nCBC	6	21.59± 0.13	1.69 ± 0.10	11.98 ± 0.07	5.27 ± 0.15	26.51 ± 5.10

4. CONCLUSION

Two groups of specimens were prepared: homogenous (CBC, mCBC, nCBC) and bimaterial specimens (bone-CBC, bone-mCBC, nbone-CBC). Tensile tests were conducted on the first group of specimens to quantify the elastic properties of cements specimens. Tension tests were conducted on the second group of specimens to quantify the MgO additive particle size effects on the interface fracture strength of bi-material specimens. This study found that MgO additives particle size positively influence the bonding strength between bone and bone cement specimens. Higher interface fracture strength was found on the bone-mCBC and bone-nCBC specimens compare to bone-CBC specimens.

5. ACKNOWLEDGMENTS

This publication was made possible by Grant Number P2PRR016478 from the National Center for Research Resources (NCRR), a component of the National Institutes of Health (NIH) and CURE-STEM faculty scholar award support from University of Central Oklahoma (UCO). Its contents are solely the responsibility of the authors and do not necessarily represent the official views of NCRR or NIH or UCO.

6. REFERENCES

1. J. E. Barralet, K. J. Lilley, L. M. Grover, D. F. Farrar, C. Ansell, and U. Gbureck, "Cements from nanocrystalline hydroxyapatite," *Journal of Materials Science: Materials in Medicine*, vol. 15, pp. 407-411, 2004.
2. G. Lewis, "Alternative acrylic bone cement formulations for cemented arthroplasties: Present status, key issues, and future prospects," *Journal of Biomedical Materials Research - Part B Applied Biomaterials*, vol. 84, pp. 301-319, 2008.
3. K. A. Mann, A. A. Edidin, N. R. Ordway, and M. T. Manley, "Fracture toughness of cocr alloy-pmma cement interfaces," *J. Biomed Mater. Res. (Applied Biomaterials)*, vol. 38, pp. 211-219, 1997.
4. K. L. Ohashi, A. C. Romero, P. D. McGowan, and M. T. Maloney, "Adhesion and reliablity of interfaces in cemented total joint arthroplasties," *Journal of orthopedic research*, vol. 16, pp. 705-714, 1998.
5. H. Liu and T. J. Webster, "Nanomedicine for

implants: A review of studies and necessary experimental tools," *Biomaterials*, vol. 28, pp. 354-369, 2007.
6. S. J. Heo, S. A. Park, H. J. Shin, Y. J. Lee, T. R. Yoon, H. Y. Seo, K. C. Ahn, S. E. Kim, and J. W. Shin, "Evaluation of bonding stress for the newly suggested bone cement: Comparison with currently used pmma through animal studies," *Key Engineering Materials*, vol. 342-342, pp. 373-6, 2007.
7. D. Khang, S. Y. Kim, P. Liu-Snyder, G. T. R. Palmore, S. M. Durbin, and T. J. Webster, "Enhanced fibronectin adsorption on carbon nanotube/poly(carbonate) urethane: Independent role of surface nano-roughness and associated surface energy," *Biomaterials*, vol. 28, pp. 4756-4768, 2007.
8. A. Ricker, P. Liu-Snyder, and T. J. Webster, "The influence of nano mgo and baso4 particle size additives on properties of pmma bone cement," *International Journal of Nanomedicine*, vol. 3, pp. 125-1, 2008.
9. Z. Shi, K. G. Neoh, E. T. Kang, and W. Wang, "Antibacterial and mechanical properties of bone cement impregnated with chitosan nanoparticles," *Biomaterials*, vol. 27, pp. 2440-2449, 2006.
10. A. Bellare, A. H. Gomoll, W. Fitz, R. D. Scott, and T. S. Thornhill, "Improving the fatigue properties of poly(methyl methacrylate) orthopaedic cement containing radiopacifier nanoparticles," Leganes, Madrid, Spain, 2003, pp. 3133-8.
11. J. Graham, M. Ries, and L. Pruitt, "Effect of bone porosity on the mechanical integrity of the bone-cement interface," *Journal of Bone and Joint Surgery-American Volume*, vol. 85A, pp. 1901-1908, 2003.
12. X. D. Wang and C. M. Agrawal, "A mixed mode fracture toughness test of bone-biomaterial interfaces," *Journal of Biomedical Materials Research*, vol. 53, pp. 664-672, 2000.

7. NOMENCLATURE

Symbol	Meaning	Unit
K_{IC}	Mode I fracture toughness	(MPa.m $^{1/2}$)
P_C	Critical load	(N)
λ	Scale factor	(unitless)
ψ	Correction factor	(unitless)
B	Thickness of specimen	(mm)
W	Width of specimen	(mm)
a	Initial crack length	(mm)
α, β	Dundurs parameters	(unitless)
E_1	Elastic moduli of cement	(MPa)
ν_1	Poisson's ratio of cement	(unitless)
E_2	Elastic moduli of bone	(MPa)
ν_2	Poisson's ratio of bone	(unitless)
h	Thickness of bone / cement in bilayer specimen	(mm)

8. MAILING ADDRESS

Morshed Khandaker
Department of Engineering and Physics,
University of Central Oklahoma,
Edmond, OK 73034, USA
E-mail: mkhandaker@uco.edu